Space Weather

RESEARCH ARTICLE
10.1029/2021SW002972

A Framework to Estimate Local Atmospheric Densities With Reduced Drag-Coefficient Biases

Vishal Ray[1], Daniel J. Scheeres[1], Suood Alnaqbi[1], W. Kent Tobiska[2], and Siamak G. Hesar[3]

[1]University of Colorado Boulder, Boulder, CO, USA, [2]Space Environment Technologies, Pacific Palisades, CA, USA, [3]Kayhan Space, Boulder, CO, USA

Key Points:

- We provide a new method to estimate accurate local atmospheric densities at sub-orbital cadence
- The biases in density and drag-coefficient are decorrelated using time-variations induced due to attitude variations in the latter
- The reduction in density bias is validated using Precision Orbit Determination data from Spire satellites

Correspondence to:
V. Ray,
vishal.ray@colorado.edu

Citation:
Ray, V., Scheeres, D. J., Alnaqbi, S., Tobiska, W. K., & Hesar, S. G. (2022). A framework to estimate local atmospheric densities with reduced drag-coefficient biases. *Space Weather*, *20*, e2021SW002972. https://doi.org/10.1029/2021SW002972

Received 29 OCT 2021
Accepted 3 FEB 2022

Author Contributions:
Conceptualization: Vishal Ray
Data curation: Vishal Ray, Suood Alnaqbi
Formal analysis: Vishal Ray
Funding acquisition: Siamak G. Hesar
Investigation: Vishal Ray
Methodology: Vishal Ray
Project Administration: Siamak G. Hesar
Resources: Vishal Ray
Software: Vishal Ray
Supervision: Daniel J. Scheeres
Validation: Vishal Ray
Visualization: Vishal Ray
Writing – original draft: Vishal Ray
Writing – review & editing: Vishal Ray, W. Kent Tobiska

Abstract An accurate estimation of upper atmospheric densities is crucial for precise orbit determination (POD), prediction of low Earth orbit satellites, and scientific studies of the Earth's atmosphere. But densities estimated using satellite tracking data are always uncertain up to the drag-coefficient assumed in the inversion method. This work develops a new framework to simultaneously estimate the density and drag-coefficient for satellites with a time-varying attitude. We do so by leveraging Fourier drag-coefficient models, previously developed by the authors, and physical models of the drag-coefficient. The method is tested with synthetic data for different geomagnetic activities, altitude levels, and errors in the gas-surface interaction parameters. We report an improvement of up to 70% in density estimates for the simulations. Finally, POD data from Spire satellites are used for validation. An improvement of around 29% is obtained in the filter density estimates over NRLMSISE-00 and 49% over JB2008 compared to the High Accuracy Satellite Drag Model densities.

Plain Language Summary With the rapidly increasing number of Earth-orbiting satellites, accurate monitoring of the satellite positions has become crucial for collision avoidance purposes. One of the major sources of error in the tracking of LEO satellites is the force that the tenuous atmosphere exerts on satellites, known as atmospheric drag. Modeling the drag force is complicated due to the uncertainties in the atmospheric density and the drag-coefficient—a parameter that governs the interactions between the atmosphere and the satellite surface. In this work, we propose a method to obtain corrections to both the density and the drag-coefficient from satellite tracking data, thus improving the tracking accuracy in the process.

1. Introduction

Atmospheric drag is the largest perturbing force for low altitude low Earth orbit (LEO) satellites. Uncertainty in its parameters, particularly atmospheric density and drag-coefficient, remains the foremost contributor of prediction errors in this orbital regime (Hejduk & Snow, 2018). In the orbit determination process, the density is usually modeled in the filter using semi-empirical models calibrated with satellite data, while the drag-coefficient is estimated as a constant. But significant discrepancies exist between the current operational semi-empirical density models (Perez & Bevilacqua, 2015) such as NRLMSISE-00 (Picone et al., 2002), JB2008 (Bowman et al., 2008) and DTM-2013 (Bruinsma, 2015), due to the differences in calibration data and physics of the models. Any errors in the atmospheric density will consequently get absorbed in the estimated states and the drag-coefficient, leading to errors in predicted orbits.

Ideally, one would minimize density errors by utilizing a model that is calibrated in real-time using tracking data from multiple satellites. An example would be the Air Force High Accuracy Satellite Drag Model (HASDM; Storz et al., 2005). Unfortunately, HASDM is not available to users outside the Department of Defense. The recently released HASDM density data set (Tobiska et al., 2021) can be used to calibrate existing semi-empirical density models. It can also be used more directly for orbit determination using a predictive framework with a chosen input parameter space (Licata, Mehta, Tobiska, et al., 2021). This can potentially result in a significant improvement in tracking and orbit predictions. But, even then, more data need to be ingested in such a framework for use across different solar cycles and during times of higher geomagnetic activity. This is especially true since HASDM densities are available at a limited spatial and temporal resolution which might not be sufficient to capture the high-frequency density variations during geomagnetic storms.

Another alternative to semi-empirical models is to use physics-based density models since they are better at capturing the thermospheric response to external forcing. But they require calibration with satellite observations of the thermosphere. Data-assimilation methods for physics-based atmospheric models have been proposed to

estimate the global atmospheric density (Matsuo et al., 2012; Sutton, 2018; Sutton et al., 2021). These methods combine the advantages of physics-based models (accounting for the thermospheric dynamics and providing density forecasts) with indirect measurements of the actual state of the thermosphere. But physics-based models don't lend themselves well to operations due to their computational complexity. This can be remedied by using reduced-order models to represent them with a smaller subset of parameters (Mehta & Linares, 2017, 2018). This technique has been used to demonstrate the estimation of global atmospheric density by assimilating measurements from accelerometers (Mehta et al., 2018), two-line element data (Gondalech & Linares, 2020), and radar and GPS measurements (Gondalech & Linares, 2021). All such data-assimilation methods significantly improve global atmospheric density estimates over existing semi-empirical models. But the obtained densities are uncertain up to the drag-coefficient assumed during the density retrieval process or estimated by the filter. Moreover, real-time tracking data from multiple sources are required to provide density estimates, which may be a hurdle for implementation in operational use. A method that can simultaneously estimate the local atmospheric density along the orbit with the drag-coefficient during orbit determination is desired. Such a method can provide near real-time corrections to the nominal density model used in the orbit determination of a satellite, unbiased by the drag-coefficient.

The simultaneous estimation of density and drag-coefficient is complicated due to their highly correlated nature. In particular, biases in the density and drag-coefficient cannot be simultaneously observed by the filter and will be estimated as a lumped term. Usually, the drag-coefficient is estimated as a constant scale factor—the so-called "cannonball drag-coefficient." The cannonball estimate averages out time-variations in the drag-coefficient due to attitude and ambient parameters and absorbs time-averaged errors in the density model. Wright and Woodburn (2004) proposed a method to simultaneously estimate the drag-coefficient and density by modeling them as exponentially decaying correlated noise terms. The drag coefficient is assumed to have a much slower variation than the density, allowing the separation of the two. This method provides a practical way to estimate the two parameters and has been used to arrive at densities derived using CHAMP and GRACE POD (McLaughlin et al., 2011, 2012; McLaughlin & Hiatt, 2008, 2009). But the bias terms in the density and drag-coefficient still cannot be estimated simultaneously, that is, the estimate is accurate only up to a constant bias. Moreover, the exponential decay model does not account for time variations in the drag-coefficient due to attitude changes. We previously developed drag-coefficient models using Fourier series expansions that account for time variations (Ray & Scheeres, 2020a; Ray et al., 2020). They have been shown to improve orbit determination and prediction for simulated and real data. We propose the use of Fourier drag-coefficient models in the simultaneous estimation of density and drag-coefficient.

This paper aims to provide a framework to estimate unbiased local atmospheric densities from satellite tracking data at a sub-orbital cadence. The time variations in the drag-coefficient induced by changes in attitude are utilized to simultaneously estimate the density and drag-coefficient. We leverage Fourier drag-coefficient models and known physics of gas-surface interactions (GSI) to estimate the bias contribution from the drag-coefficient. The higher-order time-variations in the drag-coefficient are estimated using Fourier series representations, while the density is estimated using the method proposed by Wright and Woodburn (2004). Information about uncertain GSI parameters is extracted from these Fourier coefficient estimates (Ray et al., 2021). A more accurate bias term is calculated with a better constraint on the GSI model. Therefore, with high-frequency tracking measurements such as GPS data, accurate local atmospheric density estimates along the orbit at a sub-orbital cadence are obtained for satellites with attitude variations. An improvement in the estimated densities and drag-coefficients with the proposed method is demonstrated using synthetic data across different altitudes and space weather conditions. Preliminary validation of the method is presented using POD from the Spire constellation. Sections 2 through 3 describe the datasets and methodology, while Sections 4 through 7 present the results and conclusions.

2. Data

The datasets used in this work are described as follows.

2.1. Density Data Sets

The semi-empirical density models used in this work are NRLMSISE-00 (Picone et al., 2002) and JB2008 (Bowman et al., 2008). The space weather inputs to NRLMSISE-00 are the $F_{10.7}$ index for the solar activity

level and *ap* index for the geomagnetic activity level. Both can be obtained from NOAA's website—$F_{10.7}$ at ftp://ftp.ngdc.noaa.gov/STP/space-weather/solar-data/solar-features/solar-radio/noontime-flux/penticton/ and *ap* at ftp://ftp.ngdc.noaa.gov/STP/GEOMAGNETIC_DATA/INDICES/KP_AP/. Note that NRLMSISE-00 uses the observed $F_{10.7}$ values at the actual Sun-Earth distance. JB2008 provides an improvement over previous density models by utilizing multiple space weather indices. The solar indices to JB2008 are $F_{10.7}$, $S_{10.7}$, $M_{10.7}$ and $Y_{10.7}$, and the geomagnetic indices are *ap* and *Dst*. The solar indices represent energy deposition in the thermosphere at different wavelengths. The Disturbance Storm index or *Dst* gets activated when *ap* is above 40. All the JB2008 space weather inputs can be obtained from the SET JB2008 website at https://sol.spacenvironment.net/jb2008/indices.html.

High Accuracy Satellite Drag Model densities are available as a historical data set from 1 January 2000, through 31 December 2019, that can be requested from the SET website at spacewx.com/hasdm/. The data covers two complete solar cycles with a 3-hr time resolution, at 10° × 15° latitude/longitude bins and 25 km steps between 175 and 825 km. High Accuracy Satellite Drag Model uses JB2008 as its baseline model and provides 3-hourly density corrections using 13 spherical harmonic coefficients for temperature profile parameters. These corrections are obtained using Space Surveillance Network data for more than 75 calibration objects with stable ballistic coefficients such as spherical satellites. The typical uncertainties during mean activity levels dropped from 15% for NRLMSISE-00 to around 8% for JB2008 and less than 5% for HASDM at 400 km altitude (Thayer et al., 2021). Due to these semi-empirical models' limited spatial and temporal resolution, the uncertainties can vary significantly depending on the scales and space weather activity. For example, the uncertainty around NRLMSISE-00 densities for short-term and long-scale variations is 100%. Similarly, JB2008 densities can have an uncertainty of 100% at 400–500 km for some activities and locations (ISO/FDIS 14222, 2013).

During storm conditions, using accelerometer-retrieved densities from satellites such as CHAMP and GRACE is more appropriate due to their high spatial and temporal resolution. CHAMP or the Challenging Minisatellite Payload (mission life: 2000–2010) was launched into a circular orbit with an initial altitude of 454 km. GRACE or the Gravity Recovery and Climate Experiment (mission life: 2002–2017) consisted of a pair of satellites separated by 220 km, launched into an initial orbit of 483 × 508 km. Both the missions carried highly precise accelerometers for gravity field extraction. The precise measurement of accelerations acting on the satellites has led to extensive work on atmospheric density retrieval from the onboard accelerometers and orbit tracking data. The densities derived by Mehta et al. (2017) for CHAMP and GRACE A satellites using their Response Surface Models (RSM) for the drag-coefficient are used in this work. The 2003 Halloween storm is chosen as the time epoch for simulations. The perigee and apogee altitudes for CHAMP on the chosen epoch of 29 October 2003, are 385 and 398 km, respectively. For GRACE A, the altitudes are 461 and 498 km.

2.2. Spire POD Data Set

We test the proposed method on POD from Spire satellites. Spire Global operates a constellation of over 100 CubeSats in the LEO regime with altitudes between 400 and 650 km and various inclinations. The PODs were obtained (and made available to us) by processing GNSS pseudorange and carrier phase measurements using the RTOrb software in a Kalman filtering framework. The software considers non-spherical gravity up to degree and order 120, third-body perturbations from Sun and Moon, atmospheric drag with MSISe-90 as the density model, and solar radiation pressure (SRP) with a cylindrical shadow model. Cannonball drag and SRP coefficients are estimated within each arc. The PODs obtained by RTOrb have a precision of several centimeters in position and sub-mm/s in velocity and are mostly available with a cadence of 1 s in data-arcs of 40–60 min. The attitude information of the satellites is in the form of quaternions between the body and the orbit frame. The quaternions are not uniformly available and can vary between a sample time of 10–1000 s. For our application, the quaternions are needed as frequently as possible since the Spire satellites make frequent attitude maneuvers between an observing mode with the GNSS antennas aligned along-track and a power mode where the solar flux on the solar panels is maximized. Therefore, only a small subset of the data can be used. The POD and attitude data from 7 November 2018, for satellite ID 83 is used in this work. The perigee and apogee altitudes for the satellite at the epoch are 474 and 501 km. The quaternions are interpolated to 1 s intervals using Spherical Linear IntERPolation (SLERP; Shoemake, 1985). As shown in Figure 1, the velocity vector varies significantly and frequently in the x-y plane of the body frame. The variation out of the x-y plane is negligible.

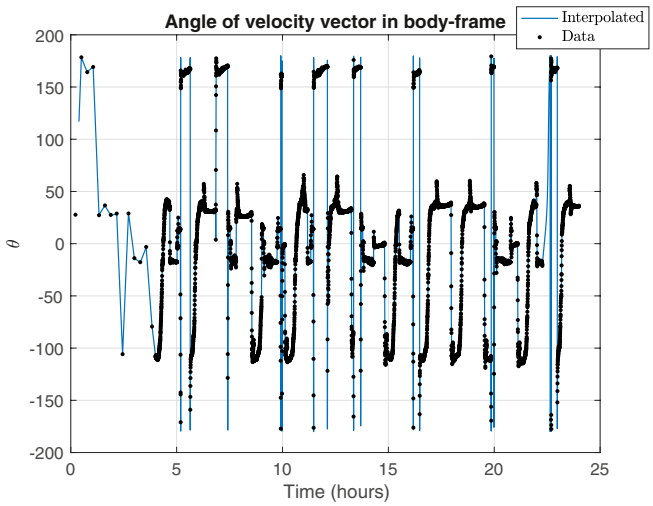

Figure 1. Angle of velocity vector with body-x axis.

3. Methodology

This section describes the different aspects of the proposed method to simultaneously estimate the density and the drag-coefficient for satellites with attitude variations.

3.1. Body-Fixed Fourier (BFF) Drag-Coefficient Model

The drag-coefficient is a function of atmospheric parameters such as molecular composition, temperature, and satellite-specific parameters such as attitude. Assuming the drag-coefficient constant in the orbit determination process, as is commonly done, introduces errors in the estimated value. But physics-based models known as gas-surface interaction models (GSIMs) that can better model the time variations have been limited in operational use due to the lack of knowledge of input parameters that feed into these models. Additionally, the drag-coefficient value can vary significantly between different GSIMs, especially at higher altitudes where the uncertainties in the GSIM parameters are larger (Bernstein et al., 2020). The Fourier series expansion models provide a way around by estimating time-variations in the drag-coefficient from tracking data. This section provides a brief overview of the Body-fixed Fourier (BFF) model that captures the drag-coefficient variations due to changes in attitude.

If the velocity vector rotates around a single axis in the body frame of the satellite, then the drag-coefficient can be expanded as a Fourier series around the angle of rotation (θ) as

$$C_d = \sum_{n=0}^{\infty} \left(\bar{\mathcal{A}}_n \cos n\theta + \bar{\mathcal{B}}_n \sin n\theta \right). \tag{1}$$

where the coefficients are given by,

$$\bar{\mathcal{A}}_n = \frac{1}{\pi} \int_0^{2\pi} C_d \cos n\theta d\theta, \tag{2}$$

$$\bar{\mathcal{B}}_n = \frac{1}{\pi} \int_0^{2\pi} C_d \sin n\theta d\theta, \tag{3}$$

for $n > 0$ and,

$$\bar{\mathcal{A}}_0 = \frac{1}{2\pi} \int_0^{2\pi} C_d d\theta, \tag{4}$$

and $\bar{\mathcal{B}}_0 = 0$ for $n = 0$.

If the satellite's attitude is known, the Fourier coefficients can be estimated in the filter using tracking data (Ray & Scheeres, 2020a; Ray et al., 2020). Initial estimates of the Fourier coefficients can be calculated by integrating a chosen GSIM in the body-frame using Equations 2–4. The integrals can be carried out numerically, but an analytical solution provides an understanding of the dependence of the different Fourier coefficients on specific GSIM parameters. This is quite useful when inverting GSIM parameters from estimated Fourier coefficients. It is possible to derive closed-form expressions for the BFF coefficients of a flat plate for the modified Diffuse Reflection Incomplete Accommodation (DRIA) model proposed by Walker et al. (2014), hereon referred to as the modified DRIA model. Ray et al. (2021) derive the analytical expressions used in this work to invert uncertain GSIM parameters from estimated Fourier coefficients.

3.2. Modeling Density Using a Gauss-Markov Process

The dynamical model used in the estimation method can have structural errors and errors in governing parameters. Static parameters can be estimated within the filtering framework, but structural errors are more difficult to compensate for. This can lead to filter divergence, where the estimation error exceeds the covariance bounds. One can remedy this by estimating the time-varying unmodeled errors as a Gauss-Markov process (GMP). A GMP is a correlated Gaussian noise such that the probability density function at the current time depends only on the probability density at the previous time instant. The unmodeled dynamics can potentially be extracted by estimating the GMP states in the filter. This is the primary motivation behind modeling the density error as a GMP in the filter.

A zeroth-order Gauss Markov process (GMP0) is equivalent to the addition of white noise. The following first-order differential equation gives the first-order Gauss Markov process (GMP1),

$$\dot{x}(t) = -\lambda x(t) + u(t), \tag{5}$$

where $E[u(t)] = 0$ and $E[u(t)u(t+\tau)] = Q\delta(\tau)$. The GMP state, $x(t)$, is augmented with the state vector and estimated in the filter. The time constant or correlation time $(1/\lambda)$ is a tuning parameter and needs to be calibrated. The first-order GMP is more accurate in compensating for errors in force models during orbit determination than simply adding white noise (Constantine & Dow, 1975). If the density error is modeled as a GMP1, it would be represented by $x(t)$ in Equation 3.

For dynamics errors with periodic components, a second-order GMP2 can prove to be more beneficial. For example, the advantage of using a GMP2 over GMP1 has been demonstrated for gravity error compensation (Leonard et al., 2013; Nievinski et al., 2011). Using GMP2 to model the atmospheric density was suggested by Nievinski et al. (2011) due to the oscillatory nature of the parameter. Gauss-Markov process can be represented in the state-space form as

$$\begin{bmatrix} \dot{x}_1 \\ \dot{x}_2 \end{bmatrix} = \begin{bmatrix} 0 & 1 \\ -\omega_n^2 & -2\zeta\omega_n \end{bmatrix} \begin{bmatrix} x_1 \\ x_2 \end{bmatrix} + \begin{bmatrix} 0 \\ c_1 \end{bmatrix} w(t), \tag{6}$$

where $E(w) = 0$ and $E[w(t)w(t+\tau)] = q\delta(\tau)$. The natural frequency of the process (ω_n), the damping factor (ζ), and the strength of the white noise (c_1 with $q = 1$) are tuning parameters that need to be calibrated. The calibration process can be performed by fitting the covariance of sample data for the modeled state to the autocovariance function of the GMP2. For example, in the case of density estimation, the sample data can be obtained from satellite missions GRACE and CHAMP or datasets such as the SET HASDM database. The fitting process doesn't always converge on the correct tuning parameters. Trial and error are usually required since significant differences between density models can be observed depending on ambient conditions. An adaptive GMP to correct for the tuning parameters using tracking data can potentially provide a better solution (Stacey & D'Amico, 2021) and will be considered in future work.

In the filter, x_1 and x_2 are both estimated and the correction to the modeled density is given by x_1. In addition to modeling the density correction using a GMP2, a GMP0 correction to the density with noise standard deviation c_2 is also estimated. The details of the filter and smoother implementation are discussed in Appendices A and B.

3.3. Simultaneous Estimation of Density and Drag-Coefficient

The drag-coefficient is usually estimated as part of the state vector during orbit determination since it is not accurately known apriori, and its value can change in orbit. If the drag-coefficient were constant, it would not be simultaneously observable with the density bias—the filter cannot distinguish between two constant terms in a product form. Any correction to one term can be easily compensated for by the other term. Therefore, with an inaccurate constant drag-coefficient in the filter, the density can be estimated only up to a bias using the methods in the previous section. But for a satellite with attitude variations, the drag-coefficient will be time-varying, as discussed in Section 3.1. Using the BFF model outlined in that section, the time-varying components of the drag-coefficient can be estimated simultaneously with the density. The bias term (zeroth-order Fourier coefficient, $\bar{A}_0$) is not observable; however, the higher-order Fourier coefficients can be estimated simultaneously with the density corrections due to the attached time-varying attitude terms. The bias in the drag-coefficient is

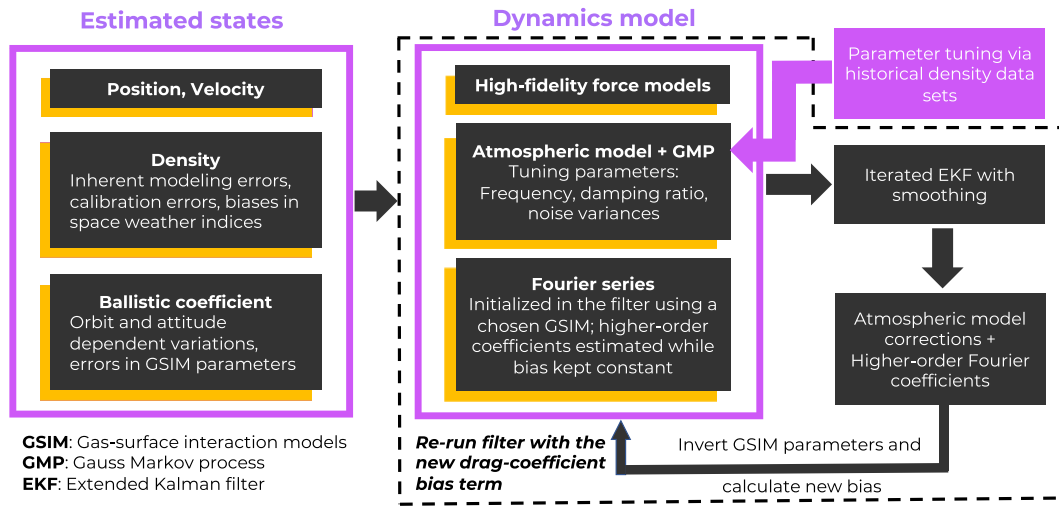

Figure 2. Summary of the algorithm.

primarily absorbed by the estimated density bias correction modeled by the GMP0. The estimated Fourier coefficients will also be affected to a lesser extent since they govern higher-order frequencies in the drag-coefficient variation that the zeroth-order term cannot capture. To calculate the drag-coefficient bias term, the functional relationship between the GSIM parameters and the Fourier coefficients represented by the integrals in Equations 2 and 3 can be utilized. A few GSIM parameters with the largest uncertainties can be inverted from the estimated Fourier coefficients (Ray et al., 2021). Then these inverted GSIM parameters can be used to calculate the zeroth-order term using Equation 4. The filter is re-initialized with the new value of the zeroth-order term, with estimates and covariances of the states from the previous iteration. A more accurate drag-coefficient bias term in the filter dynamics leads to a reduction in the density bias. The inversion process using linearized least squares is discussed in Appendix C. The algorithm (Figure 2) can be summarized as follows-

1. Initial values of the Fourier coefficients are obtained using the filter density model and the initial GSIM parameter values.
2. The Kalman filter-smoother is initialized using these Fourier coefficients. The zeroth-order Fourier coefficient or the bias term is kept constant in the filter. In contrast, the higher-order Fourier coefficients are estimated simultaneously with the satellite position and velocity, density GMP states, and other parameters.
3. A least squares method, outlined in the Appendix, is used to invert chosen GSIM parameters with the highest uncertainties from the estimated Fourier coefficients. The inverted values of the GSIM parameters are used to re-calculate the zeroth-order Fourier coefficient using Equation 4.
4. The Kalman filter-smoother is reinitialized with the new drag-coefficient bias term. All the other states are reinitialized with the estimated values and covariances from the first iteration, with the covariances slightly inflated. An improved estimate of the drag-coefficient bias leads to a more accurate density estimation.

4. Validation Using Simulated Data

This section uses controlled simulation scenarios to validate the proposed algorithm before applying it to real data. The method's performance is tested on different altitude regimes, space weather conditions, and filter model errors to understand its limitations. The true trajectories for all the cases are generated with a 10×10 geopotential (EGM-2008), a cannonball SRP model, and atmospheric drag with time-varying drag-coefficient modeled using the modified DRIA model unless otherwise stated. The modified DRIA model is given by (Walker et al., 2014)

$$C_{d,T} = f C_{d,ads} + (1 - f) C_{d,s}, \tag{7}$$

where $C_{d,ads}$ is the drag-coefficient for the surface covered by an adsorbate, assumed to exhibit diffuse reemission with complete accommodation ($\alpha = 1$). $C_{d,s}$ is the drag-coefficient based on molecular beam experiments on clean surfaces, computed using Goodman's formula for energy accommodation coefficient (Goodman &

Table 1
Summary of Simulated Cases

Case	1	2	3	4
Epoch	23 March 2007	-	29 October 2003	-
Daily F10.7	72.5	-	279.1	-
Daily Ap	10	-	204	-
Perigee/Apogee altitude (km)	360/370	510/520	385/398	461/498
True density	HASDM	-	RSM CHAMP	RSM GRACE A
Nominal filter density	NRLMSIS00	-	HASDM	-
True C_d GSIM parameters	$f = 0.7$	$f = 0.5$	$f = 0.65$, $T_w = 450$ K, JB2008 for M and T	$f = 0.5$, JB2008
Filter C_d GSIM parameters	$f = 0.98$	$f = 0.98$	$f = 0.98$, $T_w = 300$ K, NRLMSISE-00 for M and T	$f = 0.98$, JB2008
Inverted GSIM parameters	f	-	r_{ads}	f

Note. The dashes indicate that the parameters are the same as the previous column.

Wachman, 1966). The fraction of the surface covered by an adsorbate (f) is modeled using a Langmuir isotherm by Walker et al. (2014). It, therefore, is assumed to vary with the partial pressure of atomic oxygen in orbit. In this work, the fractional coverage is assumed to be steady-state since the orbits considered are nearly circular.

The densities from the SET HASDM database are used for the true density during nominally low to moderate geomagnetic activity periods. To implement the densities in orbit determination, a gridded linear interpolation of the logarithm of the densities is performed over latitude, longitude, altitude, and time. The satellite is modeled on Spire (Sutton et al., 2021) using a box-wing shape. The attitude profile is such that it tracks the Sun in light and assumes the minimal drag configuration in eclipse.

The performance of semi-empirical density models degrades during geomagnetic storms (Bruinsma et al., 2021). With the limited temporal resolution of the HASDM data set, it cannot accurately capture the time variations in density over short time scales. Therefore, to simulate the density variations during a geomagnetic storm, CHAMP and GRACE-derived densities described in Section 2 are used. To be consistent with the densities, orbital elements of CHAMP and GRACE for the given time-epoch are used to simulate the true trajectories. The simulated cases are summarized in Table 1. The symbols in the table stand for—r_{ads} is the velocity ratio for the surface covered by atomic oxygen, which is a function of the energy accommodation coefficient α and the satellite wall temperature T_w, M is the mean molar mass of the ambient gases and T is the ambient temperature. Note that the perigee/apogee altitudes are specified with respect to a mean Earth radius of 6,378.1 km.

The estimated drag-coefficients and densities for the different cases are plotted in Figure 3. For all the cases, the tuning parameters used are—$\omega_n = 0.001$ 1, $\zeta = 0.5$, $c_1 = 10^{-8}$ and $c_2 = 10^{-5}$. The natural frequency is taken as the orbit angular frequency, while the rest are chosen arbitrarily. There's a significant discrepancy between the true and nominal filter densities. NRLMSISE-00 consistently overpredicts the densities compared to HASDM during times of low geomagnetic activity, while HASDM densities are larger than the CHAMP densities during the period of the 2003 Halloween storms. After the second iteration, the estimated drag-coefficients and densities track the truth quite well for the first two cases. The density and drag-coefficient biases are reduced in the second iteration, as a better constraint on the fractional coverage parameter is obtained from the Fourier coefficient estimates.

The third case simulates a scenario where it is not apparent which GSIM parameters are the most uncertain and should be inverted. We invert the velocity ratio even though the errors are in the fractional coverage and wall temperature. Though the estimated densities track the truth (CHAMP) better than the nominal filter density (HASDM), the bias due to the drag-coefficient is not greatly reduced, as can be seen from the estimated drag-coefficient plot. The estimated densities are also not able to track the high-frequency variations visible in the truth. This is primarily because the tuning parameters are not well calibrated to model the higher-frequency variations during the geomagnetic storm. If the damping ratio is reduced and noise standard deviations increased ($\zeta = 0.09$, $c_1 = 10^{-4}$, $c_2 = 10^{-2}$), the estimated densities are able to track the temporal variations better. But in this case, the Fourier coefficients diverge from the truth, which subsequently increases the bias in the estimated densities. This

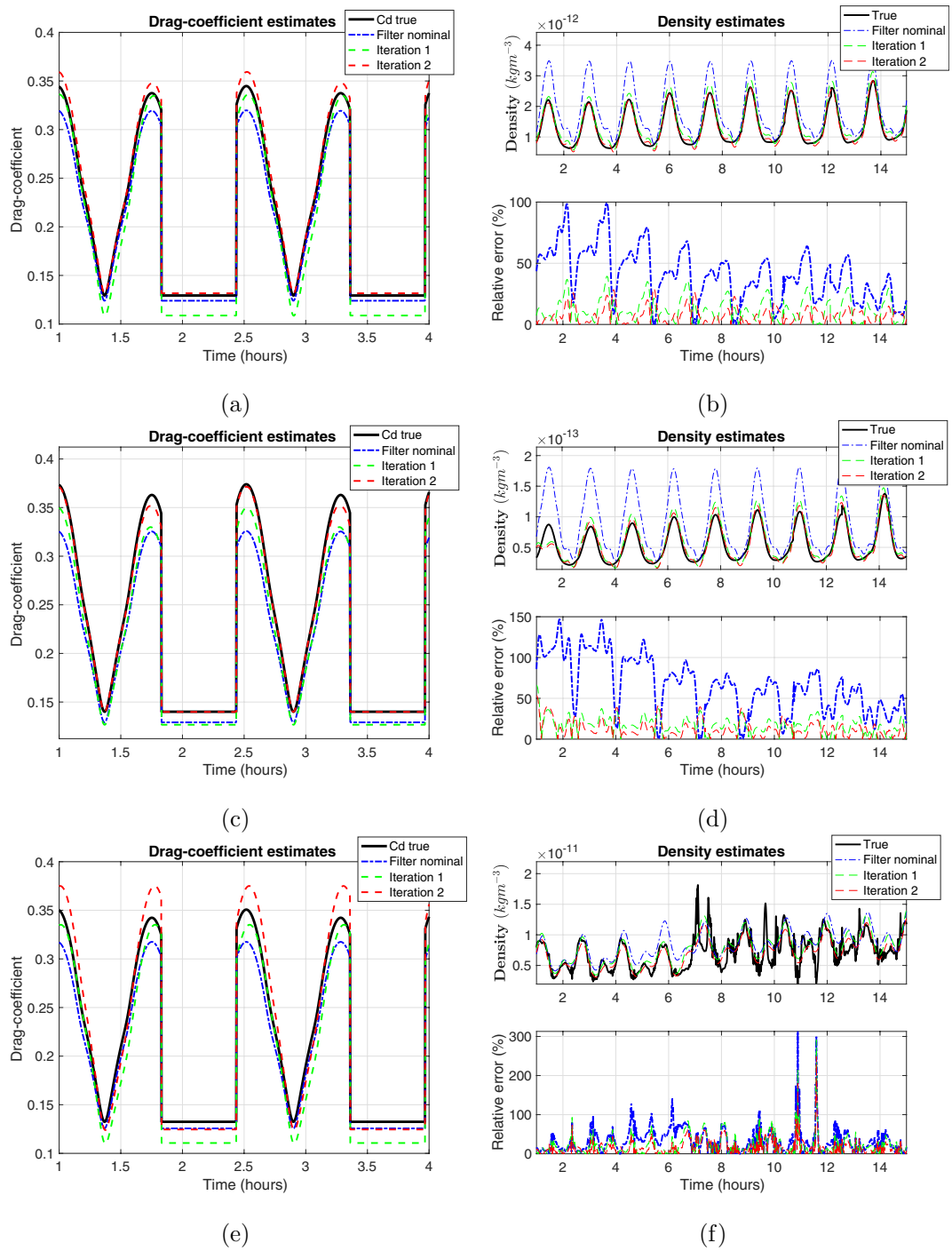

Figure 3. Drag coefficients and densities for (a), (b): Case 1, (c), (d): Case 2 and (e), (f): Case 3.

happens because the Fourier coefficient uncertainties are smaller than the noise introduced in the filter; therefore, the corrections are larger than the initial uncertainties. As seen in Figure 4a, it is better not to estimate the Fourier coefficients in this case. The estimated densities still contain the bias due to the drag-coefficient; it is more difficult to estimate the bias due to the larger noise in the filter.

There's a possible solution around the problem—modify the tuning parameters between the first and the second iterations. If low noise levels are used in the first iteration, more accurate estimates of the Fourier coefficients can be obtained though the densities do not track the time variations well. After a better constraint on the bias is

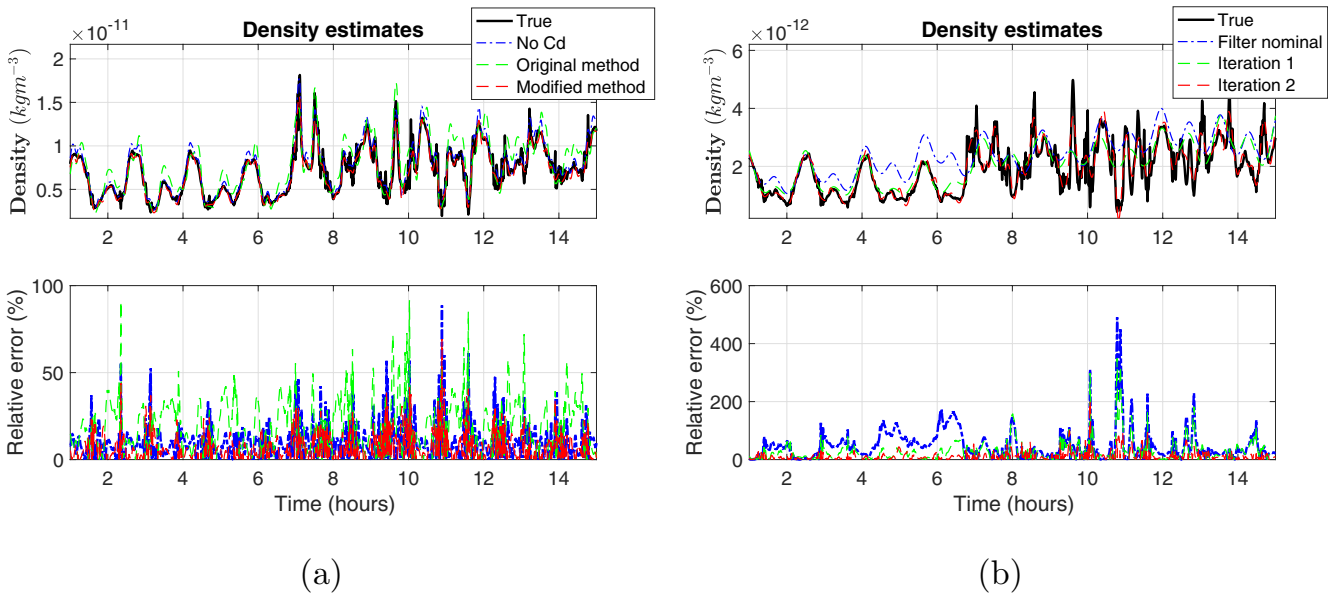

Figure 4. (a) Comparison of case 3 estimated densities for three scenarios: (1) Fourier coefficients not estimated in the filter and higher noise levels for the GMP, (2) Original method with higher noise levels for the GMP, and (3) Modified method with different noise levels between the two iterations; (b) Densities along GRACE A orbit (case 4) with the modified method.

obtained from the Fourier coefficient estimates, larger noise levels are introduced in the second iteration and the Fourier coefficients are no longer estimated. The estimated densities with this modified method accurately track the truth, as seen in Figure 4 for cases 3 and 4. It can be concluded from this example that the tuning parameters, especially the noise levels, should be selected based on the space weather activity. The mean and RMS values of the drag coefficient and density error percentages, (*truth* − *estimate*)/*truth*, are given in Table 2. In all the simulated cases, the errors in drag-coefficient and density improve compared to initial estimates after the second iteration of the algorithm. The improvement in the density estimates with the modified algorithm for cases 3 and 4 is significant.

5. Application to Spire POD

5.1. Force Model

A high-fidelity force model is required to propagate the Spire satellite orbits to isolate the orbit determination residuals solely due to errors in atmospheric drag. The forces considered in the dynamics model are given in Table 3. The initial state from the POD for a given day is propagated with the different forces to analyze the

Table 2
Mean and RMS Values of Estimated Drag-Coefficient and Density Errors (%)

		1		2		3		3 (Modified)		4	
Case		Mean	RMS	Mean	RMS	Mean	RMS	Mean	RMS	Mean	RMS
Drag Coefficient error	Initial	5.2	5.3	10.1	10.4	6.8	7	-	-	8.6	8.8
	Iteration 1	11.6	13.9	9.3	9.4	13.2	15.6	-	-	14.9	16.9
	Iteration 2	2.0	2.4	0.7	1.2	6.4	6.8	3.6	3.7	2.1	2.5
Density error	Initial	31	38.9	52.2	63	32.4	46	-	-	41.4	62.5
	Iteration 1	13	17.4	24.4	56.7	22	32.7	-	-	27.9	42.9
	Iteration 2	8.5	12.7	19.3	51.3	16.9	25.3	7.4	10.3	11.8	18.5

Note. The dashes indicate that the values are the same as the previous column.

Table 3
Forces Considered in Propagation

Force	Parameters
Non-spherical gravity	EGM-2008
	80×80
Third-body forces from Sun and Moon	DE-430 Ephemerides
Atmospheric drag	Density model - NRLMSISE-00, JB2008, SET HASDM densities Drag-coefficient- Cannonball, Panel (DRIA)
Solid Earth and Ocean tides	IERS 2010 Models (Petit & Luzum, 2010)
Solar radiation pressure (SRP)	Cannonball, Panel
Relativistic correction	Post-Newtonian correction (Montenbruck & Gill, 2000)

relative contribution of each force to the orbital states. The POD is assumed to be the "truth" to compare the propagated orbit with.

The norm of the propagated position errors (w.r.t the POD) is plotted in the upper tile of Figure 5a for the major perturbing forces with different density models for drag in the propagator. A cannonball drag coefficient is used by averaging the predicted output from the DRIA model with input parameter values of $f = 1$ and $\alpha = 0.93$, (Sutton et al., 2021) which results in a value of 0.23. The only other forces considered are non-spherical gravity (80×80) and third-body forces. High Accuracy Satellite Drag Model performs a little better than JB2008 and both are significantly better than NRLMSISE-00, as expected. In the lower tile of Figure 5a, the higher-fidelity forces are added one by one to the force model with HASDM as the density model. The addition of solid Earth tides and ocean tides leads to around 30 m improvement in the position at the end of the day, and SRP improves it further by 25–30 m. Both the forces are non-negligible when trying to isolate orbit errors due to variations in the drag-coefficient. Adding the relativistic corrections leads to a small improvement of around 2 m and changing the gravity field to order 120 improves the error by less than a metre which is barely discernible as shown in Figure 5b.

In Figure 5, the drag-coefficient is considered to be constant in the force model. But as seen in Figure 1, the relative velocity vector varies significantly in the body frame of the satellite. The propagation error with the drag-coefficient modeled using the modified DRIA model with different values of f and α are compared in Figure 6. From Figure 6a, it would seem that drag-coefficient with $f = 0$ and $\alpha = 0.93$ would provide the most accurate drag-coefficient as the propagation errors are the smallest with these parameters. But the propagation errors depend on the product of the density and drag-coefficient. It's possible that this particular drag-coefficient

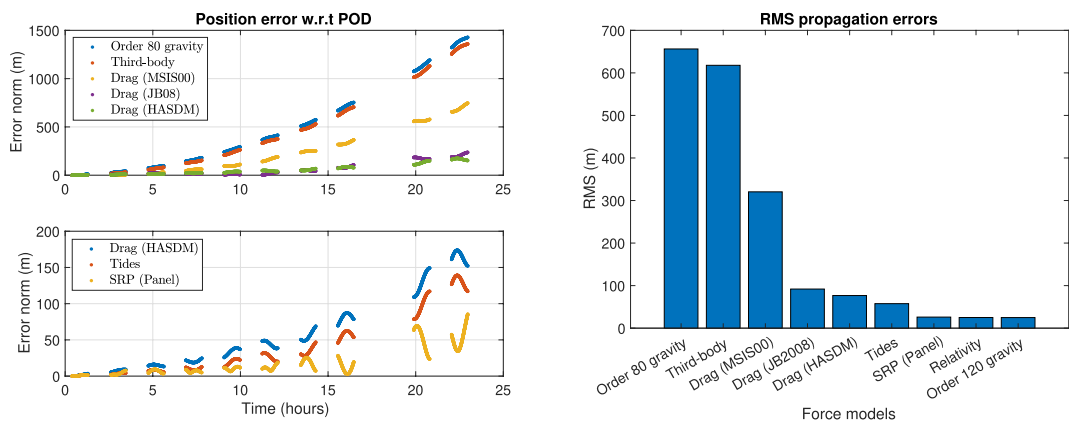

(a) (b)

Figure 5. Propagation errors w.r.t precise orbit determination: (a) Position errors with different forces added to the force model, (b) RMS of propagation errors with the addition of each high-fidelity force to the dynamics.

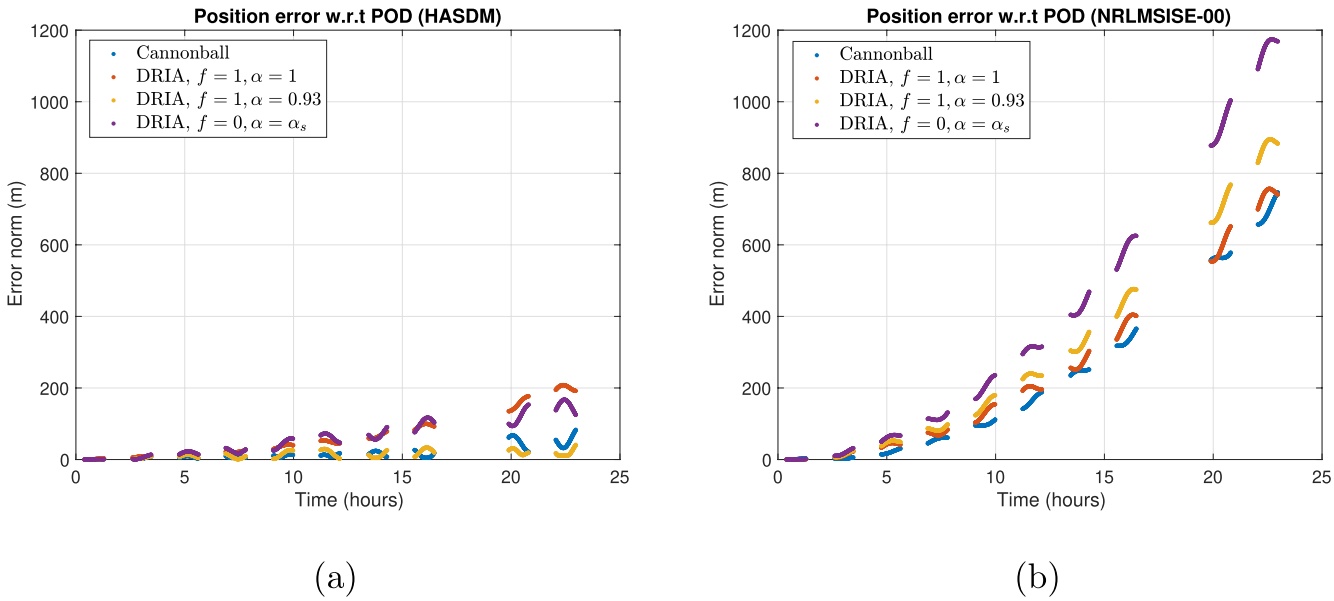

Figure 6. Propagation errors w.r.t precise orbit determination with all forces and different drag-coefficient models with: (a) HASDM as the density model, (b) NRLMSISE-00 as the density model.

model is able to compensate for the lack of spatiotemporal resolution of HASDM densities. This may result in better propagation errors even though the drag-coefficient itself is less accurate. This can be seen from Figure 6b where the propagation error trends are quite different with NRLMSISE-00 as the density model and the same drag-coefficient values. The density and drag-coefficient values from the different models are plotted in Figure 7. Note that the drag-coefficients are calculated with NRLMSISE-00 as the density model for the input ambient parameters to the modified DRIA model.

In the propagation, the SRP force model is assumed to be known accurately. The panel SRP force model is given by

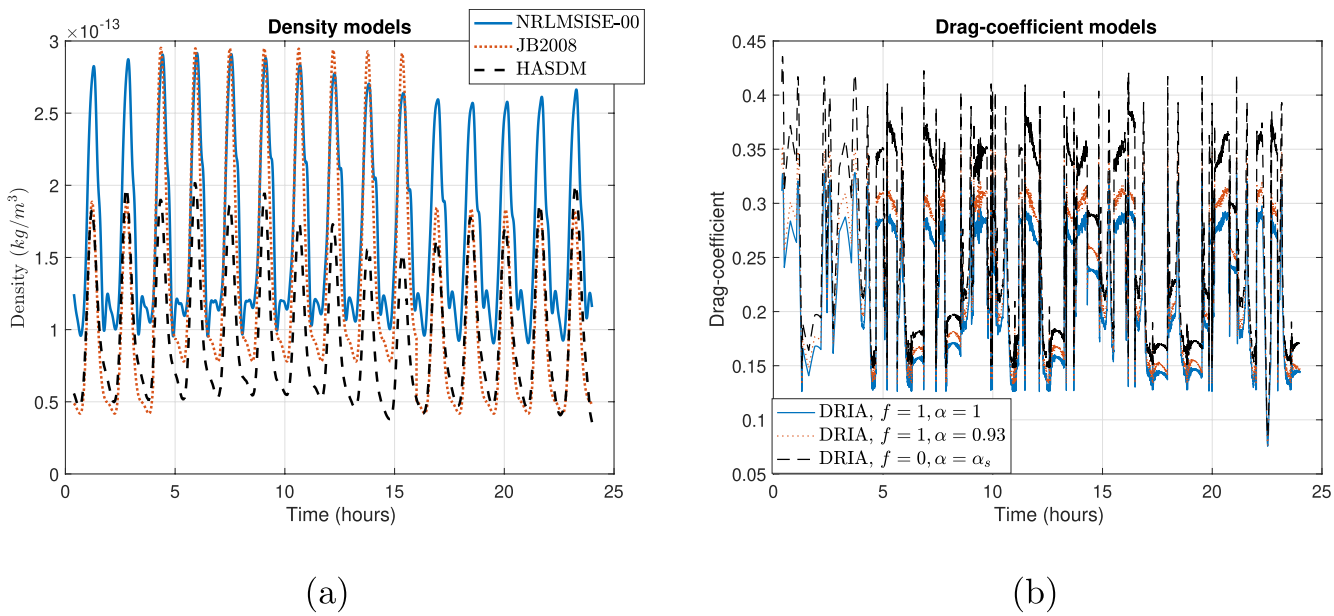

Figure 7. (a) Density values from different models, (b) Drag-coefficient values from different models.

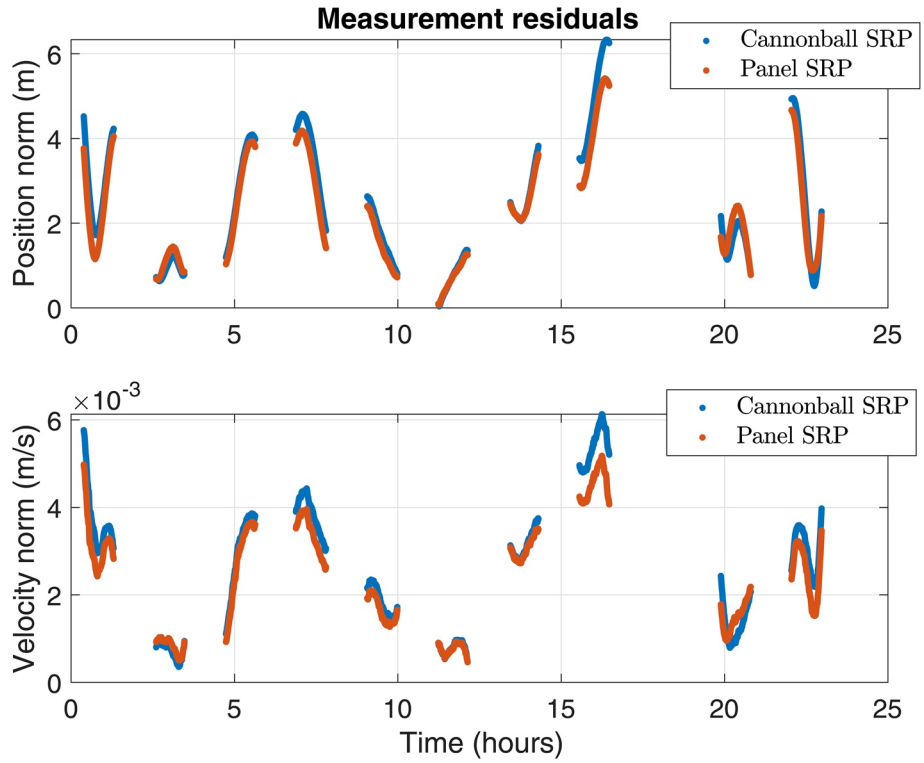

Figure 8. Measurement residuals from batch processing of precise orbit determination with two different solar radiation pressure models.

$$\boldsymbol{a_{SRP}} = -P_s \frac{C_r}{m}\left(\frac{AU}{|\boldsymbol{r_s}|}\right)^2 f_s \sum_{k=1}^{6} A_k \cos\theta_k \left[(1-\rho_k)\,\hat{\boldsymbol{r}}_s + 2\left(\frac{\delta_k}{3} + \rho_k \cos\theta_k\right)\hat{\boldsymbol{n}}_k\right]. \tag{8}$$

where $P_s = 4.56$ μPa is the SRP at 1 AU distance, $\boldsymbol{r_s}$ is the satellite to Sun position vector, f_s is the shadow factor (Montenbruck & Gill, 2000), A_k are the areas of the satellite surfaces with $\hat{\boldsymbol{n}}_k$ as the unit vectors in the satellite body frame, θ_k are the angles that the sun vector makes with the surface unit vectors, δ_k and ρ_k are the diffuse and specular reflectivities of the surfaces respectively and C_r is the SRP coefficient or the scaling factor in the panel model. The available satellite properties are assumed to be accurate in the force model with $C_r = 1$. But it is instructive to compare the orbit determination residuals for a cannonball model and the given panel model with C_r being estimated in both cases to analyze if the given panel model is indeed closer to the truth. Therefore, the POD are processed in a batch filter with all the high-fidelity force models included in the dynamics and run for the two SRP models. The initial position and velocity, cannonball drag-coefficient, and SRP coefficient are estimated, with HASDM as the density model.

Table 4
Initial and Final Estimates From the Batch Estimator for the Two SRP Models

Parameter	Initial	Final	
		Cannonball SRP	Panel SRP
Norm of position error w.r.t POD (m)	0	4.522	3.766
Norm of velocity error w.r.t POD (m/s)	0	$5.8e^{-3}$	$5.0e^{-3}$
SRP coefficient	1	0.95	0.41
Drag-coefficient	0.23	0.262	0.259

The position and velocity measurement residuals, plotted in Figure 8, are smaller for the panel model. This can be further verified from Table 4 where the correction to the initial state (which is taken to be the initial POD state) is smaller for the panel model. It is encouraging to note that the estimated drag-coefficient value is pretty much the same for either model, that is, the SRP errors don't alias into the estimated drag-coefficient (Ray & Scheeres, 2020b). The panel model with $C_r = 0.41$ is considered in the force model for the density inversion method.

The initial estimates of the Fourier coefficients are calculated using the analytical expressions for the modified DRIA model (Ray et al., 2021). The standard deviations are calculated by considering the extremities of the range of variation of the GSIM input parameters. The fraction of surface covered

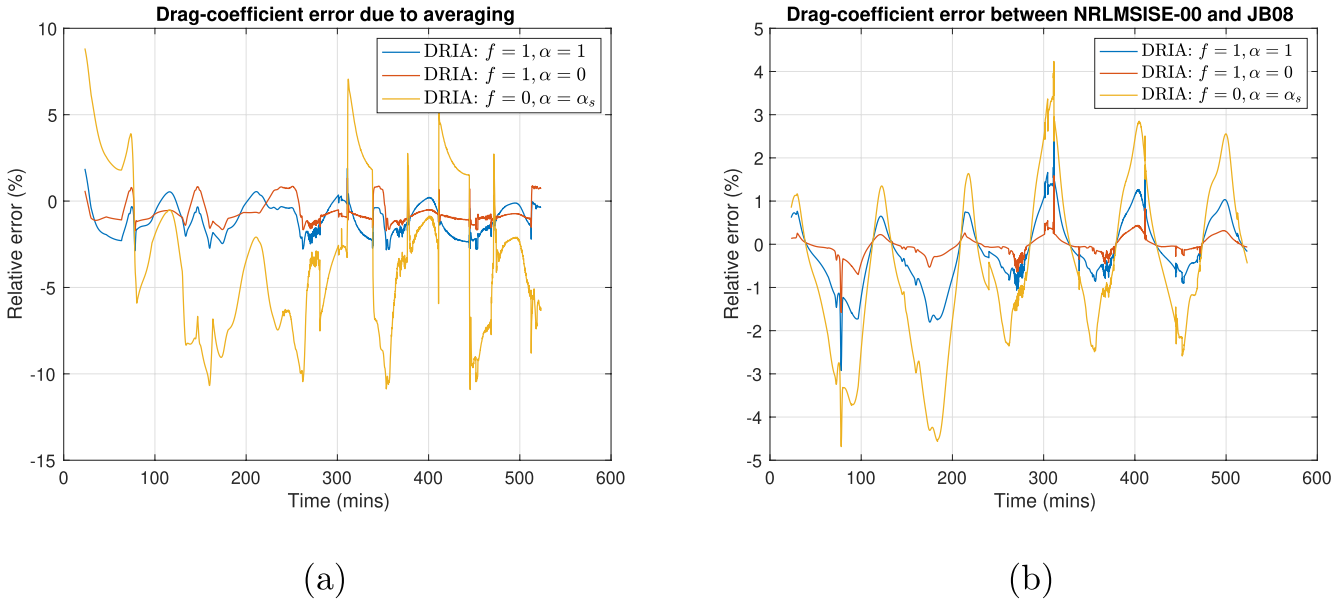

Figure 9. (a) Averaging error in the drag-coefficient, (b) Density model-dependent error in the drag-coefficient.

by atomic oxygen (f) is assumed to vary from 0 to 1 and the accommodation coefficient of the covered surface is varied from 0 to 1. The initial estimates of the body-fixed coefficients are calculated by averaging the GSIM in orbit. The initial values also depend on the density model used to provide the GSIM parameter inputs, such as the mean molecular mass. The Fourier coefficients are calculated using both NRLMSISE-00 and JB2008 for the input parameters to compare the dependence of the drag-coefficient on the density model. The effective initial drag-coefficient is calculated from the Fourier coefficients using Equation 1. The relative error introduced in the drag-coefficient due to averaging of the Fourier series expansion ($(C_{d,T} - C_{d,f})/C_{d,T}$, where $C_{d,T}$ is the modified DRIA model and $C_{d,f}$ is the orbit-averaged BFF drag-coefficient) is plotted in Figure 9a for extremal values of the GSIM parameters with NRLMSISE-00 as the density model. The relative error of the drag-coefficients calculated using JB2008 as the density model w.r.t the drag-coefficients calculated using NRLMSISE-00 as the density model is plotted in Figure 9b. Both the averaging and density model-dependent errors are within 2% when the accommodation coefficient is constant. But suppose the fractional coverage parameter is assumed to be zero and the accommodation coefficient is modeled using Goodman's formula, and therefore dependent on the density model. In that case, the relative errors are larger since now an additional parameter in the GSIM is tied to the density model.

The iterated EKF-smoother is run with the POD as measurements and NRLMSISE-00 as the density model. The state vector consists of the position, velocity, SRP coefficient, the density GMP2 states and the Fourier drag-coefficients. Only the first and second-order Fourier coefficients are estimated, while the rest of the coefficients till order 30 are kept constant in the filter. The tuning parameters for the GMP2 are found by fitting the autocovariance function to the error between NRLMSISE-00 and HASDM and then modified further by trial and error. After one iteration of the algorithm, the smoothed post-fit residuals are less than a meter in position, as seen in Figure 10a. But the estimated densities in Figure 10b are non-physical. The Fourier drag-coefficients are non-physical as well. The estimates are absorbing other periodic unmodeled dynamics errors in the orbit due to the periodic nature of GMP2 modeling.

Therefore, the density correction model is changed to a GMP1 instead, taking the time constant as the orbital period. This improves the density estimates as well as the Fourier coefficient estimates. The proposed method is used to estimate the states, with the velocity ratio (r_{ads}) inverted from the Fourier coefficient estimates. The post-fit residuals and the estimated densities from the two iterations are plotted in Figure 11. The figure also shows the density corrections when JB2008 is used as the nominal density model. It can be immediately noted that the estimated densities after each iteration move closer to HASDM, that is, the algorithm can estimate the density bias. The error statistics for the density errors w.r.t HASDM, similar to Table 1, are given in Table 5. There's

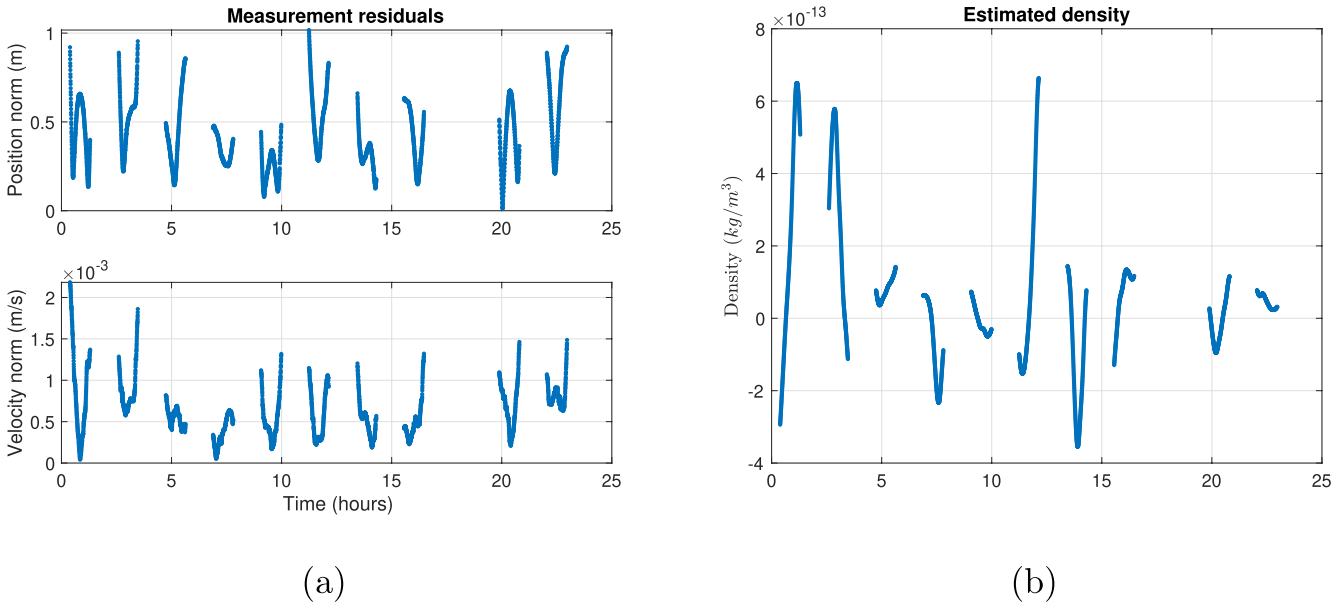

Figure 10. (a) Smoothed post-fit residuals, (b) Estimated densities from the iterated EKF-smoother.

an improvement of about 26% after the first iteration and 29% after the second iteration in the density bias with NRLMSISE-00 as the density model. With JB2008 as the nominal density model, the percentage improvement increases to 44% and 49% after two iterations respectively. It should be noted that the JB2008 densities are closer to the HASDM densities, to begin with. Although the estimated densities after both iterations are more comparable to the HASDM densities, the post-fit residuals are worse than Figure 10. Even between the iterations, the post-fit residuals are worse. However, the estimated density is closer to HASDM. This hints that remaining unmodeled dynamics are getting absorbed in the estimated densities and Fourier drag-coefficients. But even with remaining unmodeled errors, improved estimates of the density are still obtained, demonstrating the method's applicability in real scenarios.

6. Discussion

The proposed method serves to provide local atmospheric densities along a satellite orbit. The validation of this method using controlled simulation scenarios demonstrated improvements in the estimation of atmospheric densities across different altitudes and space weather conditions. The method is less sensitive to the tuning parameters used during quiet conditions, and the estimated densities track the truth accurately. However, during storm conditions, the noise levels need to be modified during the iterations. A lower noise level (similar to quiet conditions) in the first iteration ensures that the Fourier coefficients are estimated accurately. A higher noise level in the second iteration allows the estimated density to track the high-frequency variations in the true density. During the 2003 Halloween storm, the errors in HASDM are around 20%–25% around the storm period along both CHAMP and GRACE-A orbits (Licata, Mehta, Tobiska, & Huzurbazar, 2021). Using their machine-learned global temperature model called EXTEMPLAR-ML, Licata, Mehta, Wiemer, and Tobiska (2021) were able to reduce the mean density errors to 17.49% along CHAMP's orbit and 19.91% along GRACE-A's orbit. We estimate the densities to be about 10% mean using our proposed method for both the orbits. The performance of semi-empirical models such as JB2008 can degrade significantly following a storm period (Licata, Mehta, Tobiska, et al., 2021; Oliveira et al., 2021). This method can allow the densities to remain constrained within some bounds in such a scenario.

It should be noted that the lack of additional error sources contributes to the significant improvements in the estimated densities for the simulation scenarios. It would be interesting to see if such results are obtained with real data for geomagnetic storm conditions. The processing of Spire POD data during quiet conditions reveals the contribution of mismodeled dynamics and sporadic data to errors in the estimated densities. Using a lower-order error model for the density provides better results here. The estimated local densities can be used further in

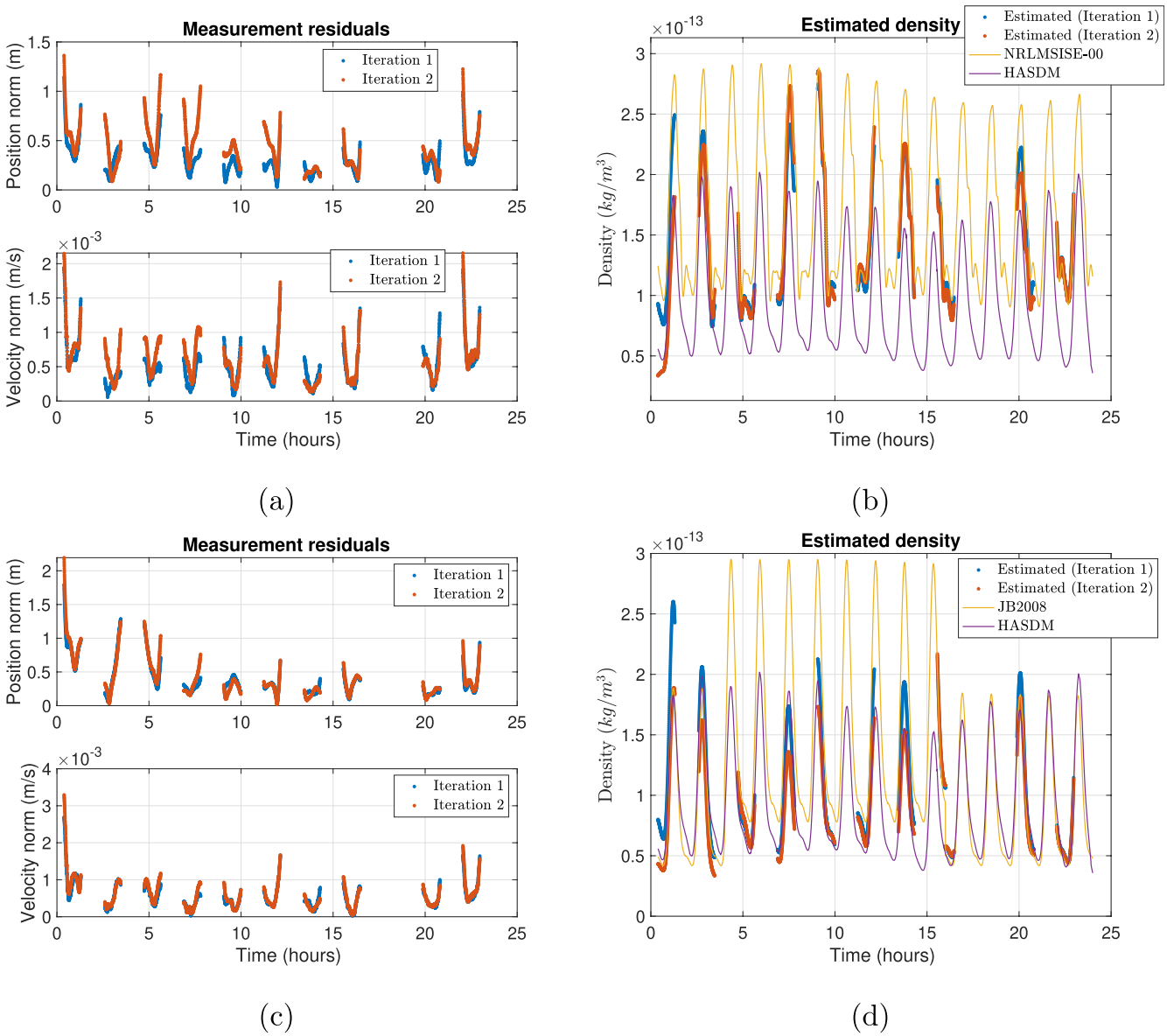

Figure 11. (a) Smoothed post-fit residuals and (b) Estimated densities from the iterated EKF-smoother with NRLMSISE-00 as the nominal density model; (c) Smoothed post-fit residuals and (d) Estimated densities from the iterated EKF-smoother with JB2008 as the nominal density model.

Table 5
Mean and RMS Values of Estimated Density Errors w.r.t HASDM Densities (%)

Iteration		NRLMSISE-00	JB2008
0	Mean	89.4	36.6
	RMS	95.5	45.5
1	Mean	65.8	20.3
	RMS	75.1	27.8
2	Mean	63.3	18.5
	RMS	73.7	26.9

Note. Iteration 0 refers to the initial errors of the nominal density model.

a data assimilation framework to calibrate existing density models. Sutton et al. (2021) estimated orbit-averaged densities using multiple Spire satellites with a fixed physics-based model for the drag-coefficient. These were further ingested in a data assimilation framework to provide global density corrections to a physics-based model. They note that using high-frequency density estimates from accelerometers provides better agreement with data with their technique. The high-frequency density estimates, corrected for the drag-coefficient biases with our proposed framework, can be a useful data source for such a method. Gondalech and Linares (2021) estimated the ballistic coefficient simultaneously with the local densities in their data-assimilation technique. But the ballistic coefficient biases had to be calculated through several-day estimation runs and corrected for the density biases. The near real-time simultaneous estimation of the ballistic coefficient bias outlined in this work can be used in such a framework.

7. Summary and Conclusions

In this work, an algorithm to simultaneously estimate the density and drag-coefficient was developed. A Gauss-Markov Process (GMP) was utilized to model the density correction in the filter. The density and drag-coefficient bias cannot be estimated simultaneously for a satellite with a constant drag-coefficient. But time-variations in the drag-coefficient due to a changing satellite attitude allow the possibility of decorrelating the two. The drag-coefficient time-variations are modeled using a Body-Fixed Fourier (BFF) expansion for a satellite with a varying attitude. The higher-order Fourier coefficients can be estimated simultaneously with the density corrections since the attitude-induced drag-coefficient signal is independent of the density variations. A few uncertain Gas-Surface Interaction Model (GSIM) parameters are inverted from the estimated Fourier coefficients in a least squares methodology utilizing the functional relationship between them, thereby providing a better constraint on the GSIM. The bias term is then re-calculated using the new GSIM parameter estimates, and the filter-smoother is rerun. The improvement in estimating the density and drag-coefficient with this algorithm was demonstrated through simulations for geomagnetically quiet and active conditions, different altitudes, and errors in GSIM parameters. The drag coefficient and density biases were reduced by more than 70% in some cases.

The algorithm was validated using Precision Orbit Determination (POD) from the Spire constellation. Even though the density correction modeled using a second-order GMP didn't converge on the truth, a first-order GMP allowed an improved density estimate. The NRLMSISE-00 density bias and error RMS w.r.t to HASDM are reduced by 26% after the first iteration and 29% after the second iteration. With JB2008 as the density model, the errors are reduced by 44% and 49%, respectively. The poor density estimate with a GMP2 suggests unmodeled periodic dynamics remaining in the filter that need further analysis. The remaining errors, such as Earth albedo and infrared radiation pressure, need to be modeled. Additionally, more dense data is required to improve the estimates. Using the POD as measurements might introduce errors due to violation of the uncorrelated white noise assumption in the Kalman filter. In the future, datasets with raw GPS measurements will be utilized for validation. As observed in one of the simulated cases, the estimates highly depend on the tuning parameters, especially the noise levels in the GMP process. Machine-learning methods can be applied to train the tuning parameters of the GMP over varying satellite orbits and atmospheric conditions using the SET HASDM database. Techniques such as adaptive GMP can dynamically change the noise levels during the filtering process. The method developed in this work can provide accurate local atmospheric density estimates at a sub-orbital cadence. It can, therefore, be used as a data-source in data-assimilation methods for density models.

Appendix A: Filter Implementation

This section outlines the implementation of GMP in an extended Kalman filter (EKF) for density estimation. The augmented state vector to be estimated is composed of the satellite position ($\boldsymbol{r}$) and velocity ($\dot{r}$), parameters ($\boldsymbol{p}$) such as the Fourier drag-coefficients and the GMP states for density correction,

$$\boldsymbol{X} = \begin{pmatrix} \boldsymbol{r}^T & \dot{r}^T & \boldsymbol{p}^T & x_1 & x_2 & x_3 \end{pmatrix}^T, \tag{A1}$$

where x_3 is the GMP0 correction and $\boldsymbol{p} \in \mathbb{R}^{m\times 1}$. The time derivative of the state vector is then given by

$$\dot{X} = \begin{pmatrix} \dot{r}^T & \ddot{\boldsymbol{r}}^T & \dot{p}^T & x_2 & -\omega_n^2 x_1 - 2\zeta\omega_n x_2 & 0 \end{pmatrix}^T. \tag{A2}$$

The density in the filter (ρ) at any time instant is given by

$$\rho = \rho_{mod}\left(1 + x_1 + x_3\right), \tag{A3}$$

where ρ_{mod} is the nominal density from an atmospheric model such as NRLMSISE-00 or JB2008 being used in the filter. Note that the corrections are normalized by the nominal density for numerical stability. The dynamics Jacobian is then given by

$$\boldsymbol{A}(t) = \begin{bmatrix} \mathbf{0}_{3\times3} & \boldsymbol{I}_{3\times3} & 0_{3\times m} & 0 & 0 & 0 \\ \frac{\partial \ddot{\boldsymbol{r}}}{\partial \boldsymbol{r}} & \frac{\partial \ddot{\boldsymbol{r}}}{\partial \dot{\boldsymbol{r}}} & \frac{\partial \ddot{\boldsymbol{r}}}{\partial \boldsymbol{p}} & \frac{\partial \ddot{\boldsymbol{r}}}{\partial x_1} & 0 & \frac{\partial \ddot{\boldsymbol{r}}}{\partial x_3} \\ \frac{\partial \dot{\boldsymbol{p}}}{\partial \boldsymbol{r}} & \frac{\partial \dot{\boldsymbol{p}}}{\partial \dot{\boldsymbol{r}}} & \frac{\partial \dot{\boldsymbol{p}}}{\partial \boldsymbol{p}} & 0 & 0 & 0 \\ \mathbf{0}_{1\times3} & \mathbf{0}_{1\times3} & \mathbf{0}_{1\times m} & 0 & 1 & 0 \\ \mathbf{0}_{1\times3} & \mathbf{0}_{1\times3} & \mathbf{0}_{1\times m} & -\omega_n^2 & -2\zeta\omega_n & 0 \\ \mathbf{0}_{1\times3} & \mathbf{0}_{1\times3} & \mathbf{0}_{1\times m} & 0 & 0 & 0 \end{bmatrix}. \tag{A4}$$

The partial of the acceleration with respect to the GMP parameters can be calculated by taking the derivative of the drag acceleration. The drag acceleration is given by

$$\ddot{\boldsymbol{r}} = -\frac{1}{2}\rho C_d \frac{A_{ref}}{m} v_r^2 \hat{\boldsymbol{u}}, \tag{A5}$$

where C_d is the drag coefficient, v_r is the relative velocity of the satellite w.r.t the atmosphere, $\hat{\boldsymbol{u}}$ is the unit vector in the relative velocity direction, m is the mass of the satellite and A_{ref} is the reference cross-sectional area. The partial can be calculated by using Equations A3 and A5,

$$\frac{\partial \ddot{\boldsymbol{r}}}{\partial x_1} = \frac{\partial \ddot{\boldsymbol{r}}}{\partial x_3} = -\frac{1}{2}\rho_{mod} C_d \frac{A_{ref}}{m} v_r^2 \hat{\boldsymbol{u}}, \tag{A6}$$

The covariance propagation for the EKF is given by

$$\boldsymbol{P}_{k+1}^{-} = \boldsymbol{\phi}_{k+1,k} \boldsymbol{P}_k^{+} \boldsymbol{\phi}_{k+1,k}^{T} + \boldsymbol{Q}_{k+1}, \tag{A7}$$

where $\boldsymbol{\phi}_{k+1,k}$ is the state transition matrix, obtained by integrating the differential equation,

$$\dot{\boldsymbol{\phi}}(t, t_k) = \boldsymbol{A}(t)\boldsymbol{\phi}(t, t_k) \qquad \boldsymbol{\phi}(t_k, t_k) = \boldsymbol{I}, \tag{A8}$$

The process noise matrix $\boldsymbol{Q}_{k+1}$ can be obtained by integrating the following equation

$$\boldsymbol{Q}_{k+1} = \int_{t_k}^{t_{k+1}} \boldsymbol{\phi}(t, t_k)\, \boldsymbol{B_a} \boldsymbol{Q_a} \boldsymbol{B_a}^T \boldsymbol{\phi}(t, t_k)^T dt. \tag{A9}$$

Here $\boldsymbol{Q_a} = \boldsymbol{I}_{3\times3}$ and

$$\boldsymbol{B_a} = \begin{bmatrix} \mathbf{0}_{(6+m)\times2} \\ \text{diag}(\boldsymbol{c}) \end{bmatrix}, \tag{A10}$$

where $\boldsymbol{c} = [c_1, c_2]$. Note that the measurement matrix does not depend on the GMP states.

Since noise is added to the states, a smoothing algorithm is implemented to reduce the error in the estimated states.

Appendix B: Iterated EKF With Smoothing

A straightforward approach to obtaining higher accuracy states in post-processing is improving past estimates using the current filtered states and measurements. The smoothing problem is finding an optimal estimate at time t_k given measurements until time t_j where $j > k$. Here we follow the fixed-interval smoothing approach (Gelb, 1974), that is, using the complete data-arc to smooth back to the past estimates. To implement this smoothing algorithm, the time histories of the state transition matrix, the process noise matrix, and the correction factor required to account for the non-linearity of the EKF need to be saved while forward filtering. The smoothing matrix is given by

$$\boldsymbol{S}_k = \boldsymbol{P}_k^{+} \boldsymbol{\phi}_{k+1,k}^{T} \boldsymbol{P}_{k+1}^{-}. \tag{B1}$$

The smoothed state $\left(\boldsymbol{X}_k^s\right)$ and state covariance $\left(\boldsymbol{P}_k^s\right)$ at the kth instant given the smoothed state at time instant $k+1$ is given by,

$$\boldsymbol{X}_k^s = \hat{\boldsymbol{X}}_k + \boldsymbol{S}_k\left(\boldsymbol{X}_{k+1}^s - \boldsymbol{\phi}_{k+1,k}\hat{\boldsymbol{X}}_k - \boldsymbol{b}_{k+1}\right), \tag{B2}$$

$$\boldsymbol{P}_k^s = \boldsymbol{P}_k^+ + \boldsymbol{S}_k\left(\boldsymbol{P}_{k+1}^s - \boldsymbol{P}_{k+1}^-\right)\boldsymbol{S}_k^T, \tag{B3}$$

where $\hat{\boldsymbol{X}}_k$ is the state estimate at the kth instant. The smoothing algorithm is initialized with $\boldsymbol{X}_N^s = \hat{\boldsymbol{X}}_N$ and $\boldsymbol{P}_N^s = \boldsymbol{P}_N^+$, where N is the number of measurements in the given data-arc. The correction factor ($\boldsymbol{b}_{k+1}$) is computed by integrating the following differential equation from t_k to t_{k+1}.

$$\dot{b}(t) = \boldsymbol{A}(t)\boldsymbol{b}(t) + \dot{X}(t) - \boldsymbol{A}(t)\boldsymbol{X}^*(t), \tag{B4}$$

with $\boldsymbol{b}(t_k) = \boldsymbol{0}$, $\boldsymbol{X}^*(t)$ refers to the propagated state estimate and $\dot{X}(t)$ is given by Equation A2. The states are smoothed back to the first time instant and the EKF with smoothing is run again with the new initial state estimate. The filter is iterated until the initial state correction drops below a certain threshold.

Appendix C: GSIM Parameter Inversion

The GSIM parameters can be inverted from the estimated Fourier coefficients using linearized least squares. In this method, the estimated Fourier coefficients are the measurements, and the GSIM parameter is the state to be estimated. The vector of Fourier coefficients have the following functional relation to the chosen GSIM parameter,

$$\boldsymbol{Y} = \boldsymbol{g}(X), \tag{C1}$$

where $\boldsymbol{Y} = \left[\bar{\mathcal{A}}_1 \ldots \bar{\mathcal{A}}_n, \bar{\mathcal{B}}_1, \ldots \bar{\mathcal{B}}_n\right]^T$, X is the chosen GSIM parameter and $\boldsymbol{g} = [g_1 \ldots g_{2n}]^T$, where g_k is the function that relates the kth Fourier coefficient to the GSIM parameter. Note that the zeroth-order Fourier coefficient is not part of the measurement vector since its estimate is not available. The following formulation demonstrates the inversion process for a generic GSIM parameter denoted as p.

The functional dependence of the kth order cosine BFF coefficient can be represented as-

$$\bar{\mathcal{A}}_k = g_k(p). \tag{C2}$$

The least squares algorithm requires the Jacobian of the measurement matrix. Therefore, $\boldsymbol{g}$ is linearized to obtain

$$\boldsymbol{G} = \left[\frac{\partial \boldsymbol{g_1}}{\partial p}, \frac{\partial \boldsymbol{g_2}}{\partial p}, \ldots \frac{\partial \boldsymbol{g_{2n}}}{\partial p}\right]^T. \tag{C3}$$

The partials can be computed analytically for the modified DRIA model since a closed-form expression for Equation C2 exists (Ray et al., 2021). But for any other GSIM, the partials can be computed numerically using the integral forms in Equations 2 and 3. Therefore, the partials are Fourier expansions of the derivative of the drag-coefficient with respect to the chosen GSIM parameter. The least squares estimate and its variance can then be found by iteratively solving the least squares equation,

$$x = \left(\boldsymbol{G}^T {\boldsymbol{R}_f}^{-1}\boldsymbol{G}\right)^{-1}\boldsymbol{G}^T {\boldsymbol{R}_f}^{-1}\boldsymbol{y}_f, \tag{C4}$$

$$P = \left(\boldsymbol{G}^T {\boldsymbol{R}_f}^{-1}\boldsymbol{G}\right)^{-1}, \tag{C5}$$

where x is the error in the estimate of the fraction at the current iteration, $\boldsymbol{y}_f$ is the measurement residual at the current iteration and $\boldsymbol{R}_f$ is the measurement noise covariance. The measurement noise covariance can be taken as the estimated covariance corresponding to the Fourier coefficients post orbit determination. The least-squares estimation process is repeated iteratively with the new estimate given by $p_{j+1} = p_j + x$, with j being the current iteration, until x drops below a fixed threshold. Once the estimate of the GSIM parameter is obtained, the bias term $\left(\bar{\mathcal{A}}_0\right)$ is calculated using the new value in Equation 4.

Data Availability Statement

The Spire POD data can be downloaded from the NASA Commercial Smallsat Data Acquisition (CSDA) Program (earthdata.nasa.gov/esds/csdap). Note that affiliation to NASA or funding through NASA is required to be able to access the data. The historical HASDM densities can be requested through the SET HASDM database (Tobiska et al., 2021; spacewx.com/hasdm/) by sending an email to data@spacewx.com with "SET HASDM density database access request" in the subject line. The CHAMP and GRACE densities derived using the RSM (Mehta et al., 2017) are publicly available at http://tinyurl.com/densitysets. The synthetic data generated for the simulations and the estimated densities from Spire POD are available in https://zenodo.org/badge/latestdoi/457054326.

Acknowledgments
This work is funded by NASA's FINESST grant under contract No. 80NSSC20K1508, and a Phase 2 STTR (F2-14919) program under contract No. FA864921P211517 with Kayhan Space Corp. We sincerely thank Eric Sutton, Senior Research Associate, SWx-TREC, CU Boulder, Shaylah Mutschler, Graduate Research Assistant, CCAR, CU Boulder, and Penina Axelrad, Joseph T. Negler Professor, CCAR, CU Boulder, for their time and effort in helping us with the Spire data set. A special thanks to Dr. James Woodburn, AGI, for his insights into their simultaneous estimation algorithm. We would also like to thank Dr. Erik Blasch, Program Officer at AFOSR, for his support.

References

Bernstein, V., Pilinski, M., & Knipp, D. (2020). Evidence for drag coefficient modeling errors near and above the oxygen-to-helium transition. *Journal of Spacecraft and Rockets*, *57*(6), 1246–1263. https://doi.org/10.2514/1.A34740

Bowman, B. R., Tobiska, W. K., Marcos, F. A., Huang, C. Y., Lin, C. S., & Burke, W. J. (2008). *A new empirical thermospheric density model JB2008 using new solar and geomagnetic indices*. AIAA/AAS Astrodynamics Specialist Conference.

Bruinsma, S. (2015). The DTM-2013 thermosphere model. *Journal of Space Weather and Space Climate*, *5*(22). https://doi.org/10.1051/swsc/2015001

Bruinsma, S., Boniface, C., Sutton, E. K., & Fedrizzi, M. (2021). Thermosphere modeling capabilities assessment: Geomagnetic storms. *Journal of Space Weather and Space Climate*, *11*(12). https://doi.org/10.1051/swsc/2021002

Constantine, P. G., & Dow, E. (1975). Dynamic model compensation for near-Earth satellite orbit determination. *AIAA Journal*, *13*(3), 343–349. https://doi.org/10.2514/3.49702

Gelb, A. (1974). *Applied optimal estimation*. The MIT Press.

Gondalech, D., & Linares, R. (2020). Real-time thermospheric density estimation via two-line element data assimilation. *Space Weather*, *18*(2), e2019SW002356. https://doi.org/10.1029/2019SW002356

Gondalech, D., & Linares, R. (2021). Real-time thermospheric density estimation via radar and GPS tracking data assimilation. *Space Weather*, *19*(4), e2020SW002620. https://doi.org/10.1029/2020SW002620

Goodman, F. O., & Wachman, H. Y. (1966). *Formula for thermal accommodation coefficient*. (M.I.T. Fluid Dynamics Research Laboratory Report). Massachusetts Institute of Technology.

Hejduk, M., & Snow, D. (2018). The effect of neutral density estimation errors on satellite conjunction serious event rates. *Space Weather*, *16*(7), 849–869. https://doi.org/10.1029/2017SW001720

ISO/FDIS 14222. (2013). *Space environment(natural and artificial)-Earth upper atmosphere*. International Standard.

Leonard, J. M., Nievinski, F. G., & Born, G. H. (2013). Gravity error compensation using second-order Gauss-Markov processes. *Journal of Spacecraft and Rockets*, *50*(1), 217–229. https://doi.org/10.2514/1.A32262

Licata, R., Mehta, P., Tobiska, W. K., & Huzurbazar, S. (2021). *Machine-learned HASDM model with uncertainty quantification*.

Licata, R. J., Mehta, P. M., Tobiska, W. K., Bowman, B. R., & Pilinski, M. D. (2021). Qualitative and quantitative assessment of the SET HASDM database. *Space Weather*, *19*(8). https://doi.org/10.1029/2021SW002798

Licata, R. J., Mehta, P. M., Wiemer, D., & Tobiska, W. K. (2021). Improved neutral density predictions through machine learning enabled exospheric temperature model. *Space Weather*, *19*(12), e2021SW002918. https://doi.org/10.1029/2021SW002918

Matsuo, T., Fedrizzi, M., Fuller-Rowell, T., & Codrescu, M. (2012). Data assimilation of thermospheric mass density. *Space Weather*, *10*(5), S05002. https://doi.org/10.1029/2012SW000773

McLaughlin, C. A., Hiatt, A., & Lechtenberg, T. (2011). Precision orbit derived total density. *Journal of Spacecraft and Rockets*, *48*(1), 166–174. https://doi.org/10.2514/1.47624

McLaughlin, C. A., Hiatt, B., & Bieber, A. (2008). Comparison of total density derived from CHAMP precision orbits and CHAMP accelerometers. *Advances in the Astronautical Sciences (AAS 08-177)*, *130*, 1193–1206.

McLaughlin, C. A., Hiatt, B., & Bieber, A. (2009). Deriving density estimates using CHAMP precision orbit data from for periods of high solar activity. *Advances in the Astronautical Sciences (AAS 09–104)*, *134*, 23–42.

McLaughlin, C. A., Lechtenberg, T., Fattig, E., & Krishna, D. M. (2012). Estimating density using precision satellite orbits from multiple satellites. *The Journal of the Astronautical Sciences*, *59*, 85–101. https://doi.org/10.1007/s40295-013-0007-4

Mehta, P., & Linares, R. (2017). A methodology for reduced order modeling and calibration of the upper atmosphere. *Space Weather*, *15*(10), 1270–1287. https://doi.org/10.1002/2017SW001642

Mehta, P., & Linares, R. (2018). A new transformative framework for data assimilation and calibration of physical ionosphere-thermosphere models. *Space Weather*, *16*(8), 1086–1100. https://doi.org/10.1029/2018SW001875

Mehta, P., Linares, R., & Sutton, E. (2018). A quasi-physical dynamic reduced order model for thermospheric mass density via Hermitian space-dynamic mode decomposition. *Space Weather*, *16*(5), 569–588. https://doi.org/10.1029/2018SW001840

Mehta, P., Walker, A., Sutton, E. K., & Godinez, H. C. (2017). New density estimates derived using accelerometers on board the CHAMP and GRACE satellites. *Space Weather*, *15*, 558–576. https://doi.org/10.1002/2016SW001562

Montenbruck, O., & Gill, E. (2000). Satellite orbits: Models, methods and applications. In *Chapter 3*. Springer. https://doi.org/10.1007/978-3-642-58351-3

Nievinski, F., Yonko, B., & Born, G. (2011). Improved orbit determination using second-order gauss-Markov process. *Advances in the Astronautical Sciences*, *140*.

Oliveira, D. M., Eftyhia, Z., Mehta, P. M., Licata, R. J., Pilinski, M. D., Tobiska, W. K., & Hayakawa, H. (2021). The current state and future directions of modeling thermosphere density enhancements during extreme magnetic storms. *Frontiers in Astronomy and Space Sciences*, *8*. https://doi.org/10.3389/fspas.2021.764144

Perez, D., & Bevilacqua, R. (2015). Neural network based calibration of atmospheric density models. *Acta Astronautica*, *110*, 58–76. https://doi.org/10.1016/j.actaastro.2014.12.018

Petit, G., & Luzum, B. (2010). *IERS conventions*. (IERS Technical Note No. 36).

Picone, J., Hedin, A., Drob, D., & Aikin, A. (2002). NRLMSISE-00 empirical model of the atmosphere: Statistical comparisons and scientific issues. *Journal of Geophysical Research*, *107*(A12), SIA 15-1-SIA 15-16. https://doi.org/10.1029/2002JA009430

Ray, V., & Scheeres, D. J. (2020a). A drag coefficient model to track variations due to attitude and orbital motion. *Journal of Guidance, Control and Dynamics*, *43*(10), 1915–1926. https://doi.org/10.2514/1.G004854

Ray, V., & Scheeres, D. J. (2020b). Gravitational force-model aliasing with non-gravitational force coefficients in dynamic prediction. *Journal of Guidance, Control and Dynamics*, *43*(10), 1984–1997. https://doi.org/10.2514/1.G005001

Ray, V., Scheeres, D. J., Hesar, S. G., & Duncan, M. (2020). A drag coefficient modeling approach using spatial and temporal Fourier expansions for orbit determination. *Journal of the Astronautical Sciences*, *67*(3), 1139–1168. https://doi.org/10.1007/s40295-019-00200-4

Ray, V., Scheeres, D. J., & Pilinski, M. D. (2021). Inverting gas-surface interaction parameters from Fourier drag-coefficient estimates for a given atmospheric model. *Advances in Space Research*, *68*(4), 1902–1927. https://doi.org/10.1016/j.asr.2021.04.010

Shoemake, K. (1985). Animating rotations with quaternion curves. In *Siggraph'85: Proceedings of the 12th annual conference on computer graphics and interactive techniques* (pp. 245–254). https://doi.org/10.1145/325334.325242

Stacey, N., & D'Amico, S. (2021). Adaptive and dynamically constrained process noise estimation for orbit determination. *IEEE Transactions on Aerospace and Electronic Systems*, *57*(5), 2920–2937. https://doi.org/10.1109/TAES.2021.3074205

Storz, M. F., Bowman, B. R., Branson, J. I., Casali, S. J., & Tobiska, W. K. (2005). High accuracy satellite drag model (HASDM). *Advances in Space Research*, *36*, 2497–2505. https://doi.org/10.1016/j.asr.2004.02.020

Sutton, E. (2018). A new method of physics-based data assimilation for the quiet and disturbed thermosphere. *Space Weather*, *10*(5), 736–753. https://doi.org/10.1002/2017SW001785

Sutton, E., Thayer, J. P., Pilinski, M. D., Mutschler, S. P., Berger, T. E., Nguyen, V., & Masters, D. (2021). Toward accurate physics-based specifications of neutral density using GNSS-enabled small satellites. *Space Weather*, *19*(6). https://doi.org/10.1029/2021SW002736

Thayer, J. P., Tobiska, W. K., Pilinski, M. D., & Sutton, E. K. (2021). Remaining issues in upper atmosphere satellite drag. In *Space weather effects and applications* (pp. 111–140). American Geophysical Union (AGU). https://doi.org/10.1002/9781119815570.ch5

Tobiska, W. K., Bowman, B. R., Bouwer, S. D., Cruz, A., Wahl, K., Pilinski, M. D., et al. (2021). The SET HASDM density database. *Space Weather*, *19*, e2020SW002682. https://doi.org/10.1029/2020SW002682

Walker, A., Mehta, P., & Koller, J. (2014). Drag coefficient model using the Cercignani-Lampis-Lord gas-surface interaction model. *Journal of Spacecraft and Rockets*, *51*(5), 1544–1563. https://doi.org/10.2514/1.A32677

Wright, J. R., & Woodburn, J. (2004). *Simultaneous real-time estimation of atmospheric density and ballistic coefficient* (Technical Report). Analytical Graphics, Inc.